One-Headed Kinesin Derivatives Move by a Nonprocessive, Low-Duty Ratio Mechanism Unlike That of Two-Headed Kinesin†

Edgar C. Young,‡ Hansraj K. Mahtani, and Jeff Gelles*

Department of Biochemistry and Center for Complex Systems, Brandeis University, Waltham, Massachusetts 02254

Received September 2, 1997; Revised Manuscript Received December 24, 1997

ABSTRACT: A single molecule of the "two-headed" motor enzyme kinesin can move along a microtubule continuously for many enzymatic turnovers (processive movement), and the velocity produced by one kinesin molecule is the same as that produced by many kinesin molecules (high duty ratio). We studied the microtubule movement driven at 1 mM ATP by biotinated N-terminal fragments of *Drosophila* kinesin heavy chain attached to streptavidin-coated coverslips at various surface densities. K448−BIO has velocity at a high density of $\bar{v}_{max} = 750$ nm s^{-1} and is dimeric (hence two-headed); K365−BIO ($\bar{v}_{max} = 200$ nm s^{-1}) and K340−BIO ($\bar{v}_{max} = 90$ nm s^{-1}) are monomeric. Escape of microtubules from the surface was prevented by methylcellulose so that continuous trajectories of microtubules not continuously attached to motor molecules could be recorded by video microscopy. The component of instantaneous velocity parallel to the microtubule axis (v) was analyzed in trajectories with a mean velocity 0.4−0.7 times $\bar{v}_{max}$. In K448−BIO trajectories, the distribution of v was bimodal with peaks near 0 and 750 nm s^{-1}. Temporal autocorrelation analysis of v detected lengthy episodes of high-velocity movement consistent with isolated processive microtubule runs driven at $\bar{v}_{max}$ by single K448−BIO dimers. K365−BIO and K340−BIO trajectories had unimodal distributions of v and autocorrelation times much shorter than those for K448−BIO. Therefore the monomeric motors have duty ratio < 55% (i.e., no forward movement is generated for at least 45% of the enzymatic cycle time) or processivity below the detection limit of ∼300 turnovers even in methylcellulose. Continuous movement at maximal velocity thus requires more than one kinesin head.

Kinesin is a motor enzyme that hydrolyzes ATP to transport organelles along microtubules (*1*). The motility of kinesin and other filament-based motors such as myosin and dynein can be studied in vitro using light microscopy: filaments can be observed gliding over enzyme-coated coverslips (*2*), or beads (*3*) or fluorescent dyes (*4*) conjugated to enzyme molecules can be observed moving along stationary filaments. A prevailing model for the movement of filament-based motors envisions that forward movement occurs in the form of a directed conformational change of the motor molecule while it is attached to the filament (a "power stroke"). The power stroke is followed by detachment from the filament and reattachment, in a mechanical cycle which is driven in one direction through coupling to the ATP hydrolysis cycle (*5*−*7*).

In principle, some reaction steps in the enzymatic cycle produce no movement, namely, those steps that occur while the motor is detached from the filament, and also chemical steps with no associated conformational change. In an extreme case, the time spent in such nonproductive reaction steps might be a large fraction of the time taken for the complete cycle. Stated in equivalent terms, the fraction of the total cycle time devoted to reaction steps that move the motor forward (called the *duty ratio*) might be low (*8*). While skeletal myosin and 22S axonemal dynein have been proposed to have low duty ratios (*9*, *10*), kinesin is an example of the other extreme, with a duty ratio close to 100%. The evidence for kinesin's high duty ratio is drawn from motility assays: a single molecule of kinesin produces processive movement (i.e., for continuous long runs on the same microtubule) at maximal velocity (*11*, *12*), and with no mechanical load and ATP not limiting, additional enzyme molecules do not increase the velocity (*11*). If one kinesin molecule spent significant time in nonproductive steps (low duty ratio), then other kinesin molecules should be able to contribute to forward movement during this time. Then, provided that a motor molecule in a nonproductive phase of the cycle did not attach to a microtubule so rigidly as to prevent all microtubule movement, the action of multiple molecules should produce a velocity higher than the velocity from a single molecule. (If a rigid inhibitory attachment were formed, the velocity from multiple molecules would be lower than that of a single molecule, as observed for kinesin at low ATP (*11*); see also ref 13.) Thus, the observation of the same maximal velocity from a single molecule and from multiple molecules indicates a high duty ratio.

A motor's duty ratio is distinct from its processivity, which is the duration of a single molecule's continuous movement,

† Supported by NIH Grant GM43369 and an HHMI Predoctoral Fellowship (to E.C.Y.).

* Address correspondence to this author at Department of Biochemistry, MS 009, Brandeis University, 415 South St., Waltham, MA 02254. Tel: (781) 736-2377. Email: Gelles@Brandeis.Edu.

‡ Current address: Center for Neurobiology and Behavior, Columbia University, New York, NY 10032.

S0006-2960(97)02172-7 CCC: $15.00
Published on Web 02/11/1998

regardless of velocity. Kinesin's high processivity implies that intervals during which kinesin is fully detached from the microtubule must be short, and indeed might not exist in typical enzymatic turnover. Since kinesin's enzymatic activity is localized to a pair of "head" regions that lie close together (*14*−*16*), alternating sites mechanisms have been proposed in which the heads take turns binding the microtubule so that the kinesin molecule as a whole translocates without detaching from the microtubule (*17*, *18*). Such mechanisms do not exclude the possibility that a single head is capable of generating some forward movement but do imply that two heads are required for specific properties of kinesin's mechanism such as high processivity and/or high duty ratio.

Some progress has been made, defining the structural determinants of kinesin motility. Kinesin is an $\alpha_2\beta_2$ heterotetramer; the heads are formed from the N-terminal residues of the heavy or α polypeptide chains (*14*, *19*) and lie at one end of an elongated α-helical coiled-coil "rod" region (*14*). K448−BIO, a recombinant biotinated derivative containing the head sequence of *Drosophila* heavy chain without the rod, forms highly stable dimers (*20*) and exhibits single-molecule processive movement like intact kinesin when attached to streptavidin beads in motility assays (*21*−*23*). The N-terminal 340 residues of the heavy chain define a highly conserved motor domain (*24*) which is monomeric (*25*); dimerization is made possible by the next approximately 40 residues of heavy chain (*26*) called the "neck" region. Dimerization is not a requirement for forward movement, since movement can be generated by K340−BIO, a monomeric biotinated derivative containing the motor domain without the neck (*22*). However, the duty ratio and processivity of monomeric motors have not been well-characterized.

In previous studies of K340−BIO, no directed movements over microtubules were observed when enzyme and beads were mixed in stoichiometric ratio (*22*). Similarly, a monomeric motor domain labeled with a fluorophore produced no observable movement events (*27*). Although the absence of events is consistent with the failure of single molecules of the motor domain to support processive movement, it might result merely from inactivation of a large fraction of the enzyme molecules in those studies. Even if the active fraction of molecules could be determined independently, studies of single-molecule movement using the bead- or fluorophore-linked assay cannot give information about the duty ratio if the motor is nonprocessive. We thus turned to the filament gliding assay; when lateral diffusion is blocked by the unbranched polymer methylcellulose (*9*), a microtubule can be observed continuously at an enzyme-coated surface even when the microtubule is not continuously associated with motor enzyme molecules. We report here measurements of instantaneous velocity of microtubule movement driven by derivatives of kinesin heavy chain attached to surfaces at low density. We used statistics-based analyses of fluctuations in instantaneous velocity to detect episodes of maximal-velocity movement from single molecules; the presence of such episodes would indicate a high duty ratio like that of intact kinesin. Although kinesin is processive, our analysis is also applicable to nonprocessive motors. In addition to the previously studied monomeric K340−BIO and dimeric K448−BIO, we tested K365−BIO, a monomeric derivative which contains 25 residues of the neck in addition to the motor domain. While our results confirm that the processive motor K448−BIO has a high duty ratio, we find that forward movement driven by small numbers of molecules of K340−BIO or K365−BIO is inconsistent with the high duty ratio and high processivity of intact kinesin. This means that a monomeric head spends a significant fraction of its turnover cycle detached from the microtubule, or else attached but occupied with reactions generating no forward movement.

Preliminary data from this work have been previously reported (*28*).

MATERIALS AND METHODS

All pH values are those measured at room temperature.

Preparation of Proteins. Calf brain tubulin and taxol-stabilized microtubules were prepared as described (*29*). K448−BIO, K365−BIO, and K340−BIO are chimeric proteins containing respectively 448, 365, and 340 N-terminal residues of *Drosophila* kinesin heavy chain. In each protein the kinesin sequence is followed by a 1−2 amino acid linker, followed by the C-terminal 87 residues of *E. coli* biotin carboxyl carrier protein. Expression of K448−BIO in Sf9 insect cell culture using the baculovirus vector system and purification by avidin affinity chromatography were performed as previously described (*20*), except that 50 nM ATP was added to all buffers to stabilize nucleotide binding sites, and avidin resin was prepared as described (*30*).

K340−BIO and K365−BIO were expressed in *Escherichia coli* BL21(DE3)(pLysS) strains and bacterial cell lysate prepared as described previously for K340−BIO (*22*). K340−BIO could also be expressed in Sf9 cells (*22*); no differences were observed between K340−BIO preparations from the two different expression hosts. K365−BIO was purified from bacterial lysate with the same avidin affinity procedure as that for K448−BIO; in some cases the final HiTrapQ chromatography step was replaced with a rapid dialysis (*31*) into storage buffer (*20*). K340−BIO did not bind efficiently to avidin affinity columns; therefore an alternative purification was employed, based on microtubule affinity (*1*). Briefly, clarified bacterial or insect cell lysate was dialyzed to remove nucleotide in excess of 50 nM ATP, clarified, and brought to 40 μM taxol, 2 mg mL^{-1} microtubules, and 1 mM AMP−PNP.[1] The microtubule−K340−BIO complex was pelleted at 20 °C (27900*g*, 30 min) through two sucrose cushions (10 and 20% (w/v) in Wash buffer (*20*) supplemented with 40 μM taxol) and resuspended at 20 °C in elution buffer (*20*) supplemented with 10 mM ATP and 40 μM taxol. Microtubules were pelleted again; the supernatant was dialyzed to remove nucleotide in excess of 50 nM ATP and chromatographed on HiTrapQ and concentrated as for K448−BIO (*20*).

Microtubule-stimulated ATPase activity of all kinesin derivatives was measured as in ref 20; typical turnover numbers in 1 mM ATP, 0.2 mg mL^{-1} microtubules were 7, 2, and 2 s^{-1} for K448−BIO, K365−BIO, and K340−BIO, respectively. Note that these numbers are not corrected for the active fraction in each preparation (*23*); moreover, the

[1] Abbreviations: AMP−PNP, adenylyl β,γ-imidodiphosphate; BSA, bovine serum albumin; EGTA, ethylene glycol-bis(β-aminoethyl ether)-*N*,*N*,*N*′,*N*′-tetraacetic acid; sd, standard deviation; se, standard error of the mean; rms, root mean square.

analyses of microtubule motility at low surface density in this work do not depend on assumptions of the value of the active fraction. All purified enzyme preparations were made 1 M in sucrose, frozen in liquid nitrogen, and stored at −80 °C with no detectable loss in activity.

Molecular Weight of K365−BIO. Diffusion coefficient measurements by gel filtration chromatography, and sedimentation coefficient measurements by sedimentation in sucrose gradients, were performed on K365−BIO as described in ref 22 and gave $D_{20,w} = 5.9 \times 10^{-7}$ cm^2 s^{-1} ($n = 1$) and $s_{20,w} \pm \text{sd} = (3.2 \pm 0.3) \times 10^{-13}$ s ($n = 4$). Molecular weight calculated as described in ref 22 was $(5.0 \pm 0.5) \times 10^4$; the monomer molecular weight predicted from the amino acid sequence is 5.0×10^4.

Microtubule Gliding. The gliding assay observed by video-enhanced differential interference contrast microscopy was adapted from (*29*). Borosilicate glass no. 0 or no. $1^1/_2$ cover slips were rinsed in ethanol and dried. Flow cells of 4−8 μL were constructed with thickness fixed by slivers of no. 0 cover slips (*11*). Solutions of 1 mg mL^{-1} biotinamidocaproyl bovine albumin ("biotin-BSA", Pierce) in 30 mM imidazole−Cl$^-$, pH 6.7, 2 mM EGTA, and 4 mM $MgCl_2$ and (as in ref 29) streptavidin (Molecular Probes), BSA (Sigma, 90% purity), and α-casein (Sigma, 85% purity) were all frozen in liquid nitrogen, stored at −80 °C, and thawed and centrifuged for 30 min at 180000*g* before use. Cells were filled with biotin-BSA and incubated for 5 min. Subsequent washes were 10 μL, and reagents were diluted in 50 mM imidazole−Cl$^-$, pH 6.7, 50 mM KCl, 2 mM EGTA, 4 mM $MgCl_2$, 2 mM dithiothreitol, and 50 nM ATP with additions noted. The cell was washed three times with 1 mg mL^{-1} BSA, once with 1 mg mL^{-1} streptavidin followed by 10 min incubation, three times with 1 mg mL^{-1} BSA, once with 0.8 mg mL^{-1} casein, once with kinesin derivative (10 pM to 1 μM) in 0.8 mg mL^{-1} casein followed by 15 min incubation, and once with 0.8 mg mL^{-1} casein, 20 μM taxol. Finally, the cell was washed with 1−10 μg mL^{-1} microtubules in 0.8 mg mL^{-1} casein, 20 μM taxol, and ATP and/or methylcellulose as desired. Methylcellulose (Sigma catalog M-0512, viscosity of 2% solution = 4000 cP at 25 °C) was used at a final concentration of 0.07% (w/w), diluted from a 2% (w/w) stock in water which was stored at −20 °C. Microtubule gliding at the coverslip surface was observed at 22−25 °C.

Microtubule Trajectory (Frame-to-Frame) Velocity Measurements. Microtubule movements were measured in video records of microscope images acquired at 30 frames s^{-1}. Sequences for movement analysis were formed by sampling frames of the video record (no averaging) at a specified rate, using image processing hardware (*32*) and customized software. Video records were usually sampled at ∼6 frames s^{-1}; some video records of microtubules moving continuously in a straight line at a velocity > 70 nm s^{-1} were sampled at 1.6−4 frames s^{-1}. The time of sampling was also recorded; hence, the *i*th frame of the sequence is associated with the time t_i relative to the time of the first sampled frame ($t_1 = 0$).

Initial data analysis is adapted from (*33*) for irregular time sequences. The position of each end of a microtubule was recorded in each frame of the sampled sequence by manual placement of a video cursor on the image of the end. For each frame at time t_i, coordinates of the ends $(x_1(t_i), y_1(t_i))$ and $(x_2(t_i), y_2(t_i))$ were used (*33*) to calculate the microtubule orientation vector $(a(t_i), b(t_i))$, the coordinates of the centroid $(x(t_i), y(t_i))$, and the microtubule length $l(t_i)$:

$$a(t_i) = x_2(t_i) - x_1(t_i), \quad b(t_i) = y_2(t_i) - y_1(t_i)$$

$$x(t_i) = \frac{x_2(t_i) + x_1(t_i)}{2}, \quad y(t_i) = \frac{y_2(t_i) + y_1(t_i)}{2} \qquad (1)$$

$$l(t_i) = [a(t_i)^2 + b(t_i)^2]^{1/2}$$

The mean value of $l(t_i)$ over the sequence was designated as the microtubule length L; the standard deviation of $l(t_i)$ was typically <5% of L. Frames in which $l(t_i)$ differed from L by more than 2.5 standard deviations were deleted from the sample sequence as momentarily unfocused or improperly digitized images; typically <2% of frames in a sequence were deleted. Frame deletion left a time gap in the sequence of remaining frames; ∼10% of sequences were truncated at the start of a gap in time of >1.4 s.

Translational displacement of the centroid between t_i and t_{i+1} was resolved into components $d_1(t_i)$ and $d_2(t_i)$, parallel and perpendicular, respectively, to the microtubule axis at t_i (*33*):

$$d_1(t_i) = \frac{b(t_i)(y(t_i+1) - y(t_i)) + a(t_i)(x(t_{i+1}) - x(t_i))}{l(t_i)}$$

$$d_2(t_i) = \frac{a(t_i)(y(t_{i+1}) - y(t_i)) - b(t_i)(x(t_{i+1}) - x(t_i))}{l(t_i)} \qquad (2)$$

Net longitudinal displacement $s_1(t_i)$ was then defined as $s_1(t_1) = 0$, $s_1(t_{i+1}) = s_1(t_i) + d_1(t_i)$ for $i \geq 1$. Mean longitudinal velocity $\bar{v}_1$ was $s_1(t_i)/t_i$ evaluated for the largest available t_i. Lateral displacement and mean velocity were analogously calculated from $d_2(t_i)$. In further analysis of longitudinal movement the direction of a complete trajectory's net longitudinal movement was used to define the "forward" direction for that trajectory. Thus, $\bar{v} \equiv |\bar{v}_1|$ is used to denote a microtubule's mean longitudinal velocity in the forward direction and is always a positive number. Values for maximal velocity $\bar{v}_{max}$ at 1 mM ATP were chosen as 90, 200, and 750 nm s^{-1} for K340−BIO, K365−BIO, and K448−BIO, respectively, through visual inspection of the values of $\bar{v}$ obtained at high surface densities of each motor enzyme.

To calculate "instantaneous" longitudinal velocity $v(t_i)$ within a short time window width w at time point t_i in a sequence, integers α and $\beta \geq 1$ were found such that $t_i - t_{i-\alpha+1} \leq w/2 \leq t_i - t_{i-\alpha}$ and $t_{i+\beta-1} - t_i \leq w/2 \leq t_{i+\beta} - t_i$. The data set of $s_1(t_j)$ at t_j for $j = i - \alpha, i - \alpha + 1, \ldots, i + \beta - 1, i + \beta$ was fitted with a least-squares regression line; $v(t_i)$ was taken as the fitted line slope, multiplied by $\bar{v}/\bar{v}_1$ (to indicate direction such that positive is forward). If no valid values of α and β existed (near the start and ends of the sequence), then no value of $v(t_i)$ was defined.

Distribution Analysis. To detect the presence of maximal-velocity movement within microtubule trajectories, distributions of instantaneous microtubule velocities were analyzed. Analysis was performed on pools of microtubule trajectories fitting the criterion $r_1 \leq \bar{v}/\bar{v}_{max} \leq r_2$, for given limits r_1 and

r_2 and for $\bar{v}_{max}$ specific to the motor in question. All available trajectories driven by the same motor and satisfying the criterion were included in the pool, regardless of the concentration of motor enzyme used to prepare the coverslip or the presence or absence of methylcellulose in the experiment. Most trajectories were recorded with methylcellulose, and $\bar{v}_{max}$ was determined from these trajectories. Inclusion of trajectories recorded without methylcellulose should not interfere with detection of velocities near $\bar{v}_{max}$, since the $\bar{v}_{max}$ of directed movement without methylcellulose is expected to be no slower than the $\bar{v}_{max}$ measured with methylcellulose.

To select an appropriate time window w for a given motor, the distribution of velocities for a "high-velocity" pool of trajectories ($r_1 = 0.85$, $r_2 = 1.15$) was examined as follows: A candidate value of w was used to calculate $v(t_i)$ in every trajectory. All $v(t_i)$ values were pooled together, and their standard deviation σ_v was calculated. The calculation was repeated for different values of w; σ_v decreased as w increased (not shown). This is expected since increasing w increases time-averaging of the data. The lowest value of w for which $\sigma_v \approx 0.33\bar{v}_{max}$ was chosen, as a compromise between the suppression of position-error noise and the detection of true fluctuations in microtubule velocity for that motor. The value of w chosen for a given motor by the above test was used for all subsequent calculations of velocity distributions for that motor. All histograms of $v(t_i)$ were prepared with a bin size of 0.04 $\bar{v}_{max}$.

Autocovariance Analysis. To characterize the duration of episodes of high-velocity movement within microtubule trajectories, the autocovariance functions of instantaneous velocities were calculated. Calculations were performed on pools of trajectories selected by motor and $\bar{v}/\bar{v}_{max}$ as for distribution analysis. For autocovariance analysis, all $v(t_i)$ data were calculated using $w = 500$ ms regardless of motor identity. This choice of w corresponds to minimal time-averaging, with typically five time points used in each $v(t_i)$ calculation. $C(\tau)$, the temporal autocovariance of $v(t_i)$ for the pool of trajectories, was calculated for $\tau = (1000n - 500)$ ms for integer $n \geq 1$ as follows: For each trajectory, the functions $F(\tau)$ and $G(\tau)$ were evaluated at each τ by the summations

$$F(\tau) = \sum_{t_i,t_j}\left[\frac{(v(t_i) - \bar{v})(v(t_j) - \bar{v})}{(\bar{v}_{max}/2)^2}\right] \qquad G(\tau) = \sum_{t_i,t_j} 1 \tag{3}$$

taken over all pairs (t_i,t_j) in the trajectory data set for which $\tau - 500$ ms $\leq (t_j - t_i) < \tau + 500$ ms. $F(\tau)/G(\tau)$ is the autocovariance of $2v(t_i)/\bar{v}_{max}$ in the single trajectory; its intercept $F(0)/G(0)$ is $4(\sigma_v/\bar{v}_{max})^2$. $C(\tau)$ was taken as the weighted average of the individual trajectory autocovariances at each τ:

$$C(\tau) = \frac{\sum F(\tau)}{\sum G(\tau)} \tag{4}$$

where the sums were taken over all trajectories.

For microtubule-length-normalized autocovariance analysis, each trajectory's $v(t_i)$ data set was reparametrized to use the dimensionless $\delta_i = t_i\bar{v}_{max}/L$ as the independent variable. Calculations analogous to those above were made with bin size 0.05, i.e., with $\Delta = 0.05n - 0.025$ for integer $n \geq 1$. Specifically, for each trajectory the functions $F(\Delta)$ and $G(\Delta)$ were evaluated at each Δ by the summations:

$$F(\Delta) = \sum_{\delta_i,\delta_j}\left[\frac{(v(\delta_i) - \bar{v})(v(\delta_j) - \bar{v})}{(\bar{v}_{max}/2)^2}\right] \qquad G(\Delta) = \sum_{\delta_i,\delta_j} 1 \tag{5}$$

taken over all pairs (δ_i,δ_j) in the trajectory data set such that $\Delta - 0.025 \leq (\delta_j - \delta_i) < \Delta + 0.025$. Then the microtubule-length-normalized correlation $C_N(\Delta)$ of pooled trajectories was evaluated at each Δ:

$$C_N(\Delta) = \frac{\sum F(\Delta)}{\sum G(\Delta)} \tag{6}$$

where the sums were taken over all trajectories.

Estimate of Position-Error Noise. Misestimation of microtubule end positions due to variation in the placement of video cursors is the dominant source of error in the microtubule velocity measurements. The magnitude of the noise introduced by such errors was estimated from experimental trajectories of continuous microtubule gliding at 1 mM ATP driven by K340−BIO with $\bar{v} > 76.5$ nm s^{-1} or by K448−BIO with $\bar{v} > 637.5$ nm s^{-1}. (These lower limits correspond to $0.85\bar{v}_{max}$ for each enzyme.) Each trajectory's rms position noise was estimated as the standard deviation of $(s_1(t_i) - \bar{v}_1 t_i)$ over the trajectory; this is an upper limit to the true noise because it assumes no variation in microtubule velocity during continuous high-velocity gliding. The mean value (±sd) of the rms position noise over all trajectories was 148 ± 48 nm ($n = 18$) for K340−BIO and 180 ± 84 nm ($n = 17$) for K448−BIO.

Simulated Trajectories for the High Duty Ratio Model. For a direct comparison of experimental trajectory data with predictions of a high duty ratio model, trajectories consistent with the model were numerically simulated. The simulations assumed that each of the three kinesin derivatives has complete processivity and a duty ratio near 100% and differ only in that $\bar{v}_{max} = 750$ nm s^{-1} for K448−BIO, 200 nm s^{-1} for K365−BIO, and 90 nm s^{-1} for K340−BIO. Simulated microtubule trajectories were constructed on the basis of a model in which single molecules of a given motor are randomly distributed on the surface at very low density so that a diffusing microtubule encounters and forms attachment to only one motor molecule at a time. During diffusion, encounter events occur with a probability independent of time (a Poisson process); diffusion ends after an encounter event. Directed movement begins with the encounter event (at a random point along the microtubule length) and proceeds at $\bar{v}_{max}$ from the initial attachment point to the plus-end of the microtubule; diffusion resumes when the plus-end is reached. For each simulated trajectory, a microtubule length L was chosen randomly from a Gaussian distribution with mean (±sd) = 4.0 ± 3.0 μm. Lengths <1 μm were discarded,

resulting in a length distribution (mean 4.6 ± 2.1 μm, sample of 60 simulations) resembling that of experimental data (e.g., 4.4 ± 1.9 μm, $n = 86$ for K340−BIO experiments). In each simulation a noiseless trace of net longitudinal displacement at time t_i was generated as a discrete function $s_0(t_i)$, with time points every $\Delta t = 166$ ms and $s_0(t_1) = 0$. Each trace was composed of a series of six consecutive episodes (sets of contiguous time points), with three "diffusing" and three "directed" episodes in strict alternation. The duration of each directed episode was chosen randomly from a flat distribution bounded by 0 and $L/\bar{\nu}_{max}$. The duration of each diffusing episode was chosen randomly from a Poisson interval (exponential) distribution (*34*) with mean $0.5L/\bar{\nu}_{max}$. Thus over many simulations $\bar{\nu}/\bar{\nu}_{max}$ had an average value ≈0.5, and complete trajectories had a mean duration $\approx 3L/\bar{\nu}_{max}$; this resembled the intermediate velocity pools of experimental trajectories ($0.4 \leq \bar{\nu}/\bar{\nu}_{max} \leq 0.7$) which had mean durations of 22 (K448−BIO), 69 (K365−BIO), and 132 s (K340−BIO). For each time point t_{i+1} of a directed episode, $s_0(t_{i+1})$ was set to $s_0(t_i) + \bar{\nu}_{max}\Delta t$. For each time point t_{i+1} of a diffusing episode, $s_0(t_{i+1})$ was set to $s_0(t_i) + d_{diff}$, where d_{diff} was chosen randomly from a Gaussian distribution with mean 0 and variance $2D_{long}\Delta t$, with D_{long} set as described below in *Estimates of Microtubule Diffusion Coefficient*. Then a noise-added displacement data set $s_1(t_i)$ was constructed: for each time point t_i of the trajectory, $s_1(t_i)$ was set to $s_0(t_i) + \epsilon_{noise}$, where ϵ_{noise} was chosen randomly from a Gaussian distribution with mean 0 and sd 150 nm to simulate position-error noise. Batches of 15−60 simulated $s_1(t_i)$ data sets for a given motor were subjected to the same analyses (i.e., with the same values of w as those used in the distribution and autocovariance analysis) as experimental $s_1(t_i)$ sets for that motor.

Estimates of Microtubule Diffusion Coefficient. The microtubule diffusion coefficient (D_{long}) for use in simulations was determined from trajectories of microtubules diffusing in methylcellulose over surfaces with no motor enzyme attached. For each recorded trajectory the $\nu(t_i)$ values were calculated with w as noted below, and the rms displacement for longitudinal diffusion was estimated as the standard deviation of $\nu(t_i)w$. The diffusion coefficient D for the trajectory was estimated by assuming that rms displacement $= (2Dw)^{1/2}$ based on the diffusion equation (*34*). D was calculated for $w = 1$, 3, 6, and 10 s; no systematic variation was found, and in each trajectory the four values had sd < 30% of their mean. The mean of the four values was then designated as the trajectory's longitudinal diffusion coefficient D_{long}. D_{long} decreased with microtubule length L; for 13 microtubules with mean (±sd) $L = 5.0 \pm 2.0$ μm (range of 2.7−8.5 μm), D_{long} had mean (±sd) $= (9.9 \pm 5.0) \times 10^4$ nm^2 s^{-1}.

When simulations of completely processive, high duty ratio motors were performed using $D_{long} = (5-25) \times 10^4$ nm^2 s^{-1}, histograms of ν in the distribution analysis of simulated trajectories with intermediate or low $\bar{\nu}/\bar{\nu}_{max}$ were wider than the corresponding experimental histograms. In particular, the width of the peak centered at zero (corresponding to diffusion episodes) in each simulation histogram was far greater than the entire experimental histogram width. The discrepancy between simulation and experiment could be quantified by calculating the standard deviation of ν, σ_ν, which was 15−150% higher for simulation histograms than for the corresponding experimental histograms. In contrast, when D_{long} was set to $(0.1-1) \times 10^4$ nm^2 s^{-1}, the difference between σ_ν values of simulation and experiment was <10% for all three motors. Undirected longitudinal motion over surfaces with motors attached is thus considerably more restricted than microtubule diffusion over motor-free surfaces. The undirected movement within experimental K448−BIO trajectories is believed to represent free longitudinal diffusion over K448−BIO-coated surfaces. We attribute the discrepancy between D_{long} estimated from undirected movement over K448−BIO-coated surfaces ($\sim 1 \times 10^4$ nm^2 s^{-1}) and D_{long} measured for diffusion over motor-free surfaces ($\sim 1 \times 10^5$ nm^2 s^{-1}) to a smaller mean distance between microtubules and the coverslip in the former experiments. An increase in the frictional drag coefficient is expected for a microtubule very close to the surface (*35*). Therefore the simulations that were intended for comparison with experimental results in autocovariance analysis of motor-driven movement were generated with a longitudinal diffusion coefficient $D_{long} = 1 \times 10^4$ nm^2 s^{-1}.

RESULTS

Microtubule Movement Driven by Kinesin Derivatives with and without Methylcellulose. Biotinated motor enzymes can be attached specifically to streptavidin-coated surfaces in a constant orientation to facilitate motility assays (*22*, *29*). Each of the kinesin derivatives K448−BIO (dimeric) and K365−BIO and K340−BIO (monomeric) drove unidirectional microtubule gliding in the presence of 1 mM ATP, if the concentration of motor incubated with the streptavidin-coated coverslip (see Materials and Methods) was ≥50 nM. Gliding in such experiments was continuous and parallel to the microtubule axis and occurred over distances greater than the microtubule length.

Experiments were repeated using successively lower motor concentrations in the incubation protocol; this lowers the surface density of attached motors. Initially experiments were performed without methylcellulose. K448−BIO produced observable movement events even when the K448−BIO concentration in the incubation was reduced to picomolar levels. A microtubule often appeared to "pivot" around, and move through, a single point of attachment to the surface, as observed for microtubules driven by single molecules of intact kinesin (*11*). When the trailing end of the microtubule passed through the pivot point, the microtubule diffused away from the surface, ending the observation. In contrast, coverslips incubated with ≤10 nM K365−BIO or ≤1 nM K340−BIO did not produce observable microtubule movement events in 1 mM ATP. Although microtubules formed transient contacts with the surface, they diffused away from the surface within 1 s. This was not simply because the coverslips incubated with low motor concentrations had no motors attached: in control experiments, microtubules did form long-lived attachments to the same coverslips when the ATP concentration was only 50 nM, whereas microtubules in 50 nM ATP did not attach to coverslips which had not been incubated with any motor.

Because rapid escape of microtubules away from the surface would preclude analysis of directed movement, the unbranched polymer methylcellulose was introduced into the motility assay to hinder microtubule diffusion in the direction

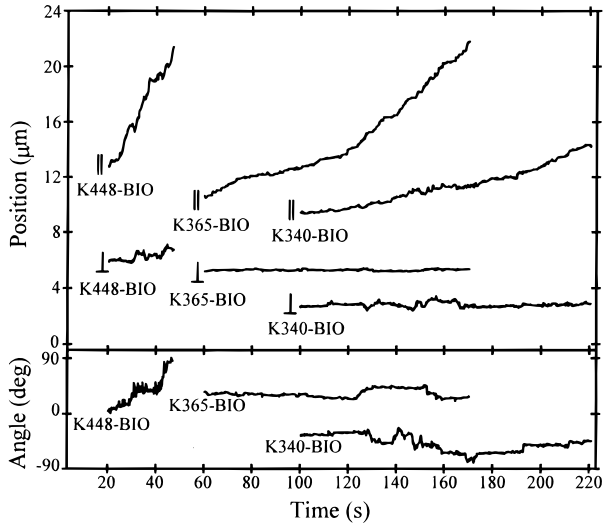

FIGURE 1: Components of motion extracted from trajectories of microtubules driven at 1 mM ATP by kinesin derivatives attached to coverslips at low surface density. Individual microtubules were observed in the presence of 0.07% methylcellulose, moving over streptavidin-coated coverslips which had been incubated with solutions containing either 0.051 nM K448−BIO, 10 nM K365−BIO, or 0.84 nM K340−BIO. One microtubule trajectory for each motor was selected for this figure. Frame-to-frame displacement of microtubule centroid was resolved into components parallel (||) or perpendicular (⊥) to the microtubule axis. Each microtubule trajectory is represented by three traces (net displacement parallel and perpendicular to axis, and microtubule orientation); the origin along the horizontal axis for each set of three traces is arbitrary, as are origins of all traces along the vertical axis.

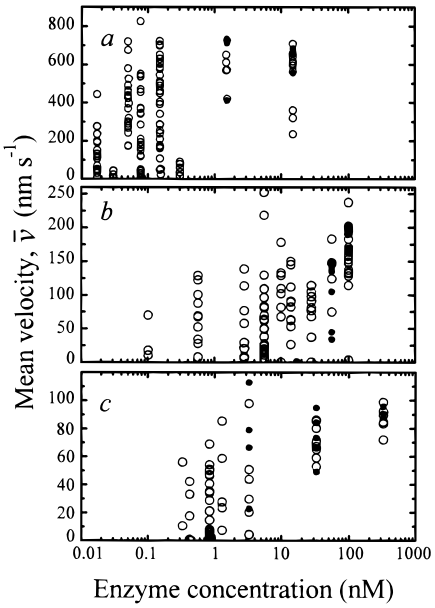

FIGURE 2: Mean longitudinal velocities of individual microtubule trajectories produced at 1 mM ATP by different kinesin derivatives. Streptavidin-coated coverslips were incubated with solutions containing K448−BIO (a), K365−BIO (b), or K340−BIO (c) at the indicated enzyme concentrations. Each point shows $\bar{v}$ (net displacement parallel to microtubule axis divided by total time) for an individual microtubule trajectory, observed with (○) or without (●) 0.07% methylcellulose.

perpendicular to the surface. In methylcellulose solutions, microtubules near the surface moved primarily within a plane close to the surface for up to 200 s and thus remained in focus as they explored different regions of the surface. From the video record of a microtubule movement trajectory, the frame-to-frame movement of the microtubule was resolved (*33*) into a translation of the microtubule centroid (with displacement components parallel and perpendicular to the microtubule axis) and a change in microtubule angle. In control experiments in which no motor at all was incubated with the coverslip, all components of movement appeared random. The diffusion coefficient for longitudinal movement (parallel to the microtubule axis) was (0.5−2.5) × 10^5 nm^2 s^{-1} (depending on microtubule length); by comparison, the longitudinal diffusion coefficient calculated for a cylinder of 4 μm length and 25 nm diameter in water without methylcellulose (viscosity 1 cP) is 8 × 10^5 nm^2 s^{-1} (*34*). Thus, although the methylcellulose suppressed virtually all diffusion perpendicular to the surface, it had only a small effect on longitudinal diffusion.

In trajectories of microtubules moving over surfaces with motors attached at low density (Figure 1), the angle change and lateral displacement appeared random, but the net longitudinal displacement displayed systematic movement, usually >2000 nm over the trajectory. Although some reversals in direction were observed, particularly in experiments with very low motor surface density, instances of sustained movement in one direction were usually all in the same direction within a trajectory. This is consistent with motor-driven movement in a direction determined solely by microtubule polarity.

For the monomeric motors, the use of methylcellulose lowered the minimum motor surface density for which directed microtubule movement could be observed. Trajectories with significant net longitudinal displacement were observed over coverslips treated with nanomolar or subnanomolar concentrations of the monomeric motors, i.e., at surface densities too low for observing movement events without methylcellulose. This suggests that, in the experiments without methylcellulose, the monomeric motors were indeed active but simply could not maintain continuous contact with a microtubule during extended episodes of movement.

For each microtubule trajectory, the mean velocity ($\bar{v}$, net forward longitudinal displacement divided by total trajectory time) was calculated. In experiments with high concentrations of motor applied to the coverslip, $\bar{v}$ values clustered around a saturating $\bar{v}_{max}$ specific to each motor. With lower concentrations, the distribution of $\bar{v}$ values broadened as many trajectories had $\bar{v} < \bar{v}_{max}$ (Figure 2). No systematic dependence of $\bar{v}$ on microtubule length was observed in the range 1−14 μm (not shown). Estimates of $\bar{v}_{max}$ from Figure 2 were 750 nm s^{-1} for K448−BIO, 200 nm s^{-1} for K365−BIO, and 90 nm s^{-1} for K340−BIO. The turnover time of K448−BIO in 1 mM ATP is ∼10 ms (*23*); if the distance traveled per turnover cycle by a monomeric motor is similar to the 7 nm width of the kinesin head (*36*) or the 8 nm step of K448−BIO (*23*), then the $\bar{v}_{max}$ values suggest that K365−BIO and K340−BIO have turnover times in the motility assays of ≤100 ms. To ask whether methylcellulose produced significant frictional drag on the longitudinal movement of microtubules, experiments using high motor concentration with and without methylcellulose were compared. The values of $\bar{v}$ for trajectories with and without methylcellulose were similar (Figure 2).

Rationale for Duty Ratio Measurement Techniques. At each point in a microtubule's movement trajectory, the (essentially) instantaneous velocity v of longitudinal movement can be calculated from the microtubule position data in a time window of short duration w. If w is significantly longer than the motor's enzymatic turnover time of 10−100 ms, then v is influenced by the mean number of motor molecules performing turnover cycles that contribute to microtubule movement during the time window, as well as the velocity of movement produced by an individual motor molecule during a complete turnover cycle. Because methylcellulose in the gliding assay hinders the diffusive escape of microtubules from the surface, a motor molecule close to a microtubule has a high probability of maintaining this proximity through successive turnovers, even if the motor detaches momentarily during turnover. Thus, it is likely that methylcellulose will increase the processivity of a motor which is nonprocessive in the absence of methylcellulose. (The exception is in cases where the motor enters some state that cannot interact with a microtubule for a prolonged time, so that the restriction on microtubule diffusion by methylcellulose is insufficient to ensure that the motor reattaches to the same microtubule.) In cases where methylcellulose does render the motor capable of processive movement, then the number of motor molecules participating in movement will tend to remain constant on the time scale of individual turnovers. However, the number of motors will fluctuate on a time scale slower than the turnover time, as the microtubule moves over regions of the surface with slightly different motor densities. Hence, the instantaneous velocity during the trajectory, v, will fluctuate around the mean $\bar{v}$. We presume that each trajectory with submaximal mean velocity arises because in that trajectory the microtubule samples a region of coverslip surface with low active motor density; the local density in this region may differ from the average over the coverslip. Thus, for each of the three motors studied, data from trajectories with similar $\bar{v}/\bar{v}_{max}$ were pooled, regardless of the nominal motor concentration applied to the coverslip in the experiment.

Microtubule gliding driven by a high duty ratio motor like intact kinesin has distinctive features. For such a motor, microtubule gliding occurs at velocity $v = \bar{v}_{max}$ as long as *any* nonzero number of active motor molecules contribute to movement (*11*). Microtubule movement will be random (zero average velocity) when no motors are attached. Thus, movement slower than $\bar{v}_{max}$ occurs only when the microtubule reaches a region of the coverslip surface with no motors close enough for attachment. At sufficiently low surface density of molecules of a high duty ratio motor, a microtubule will undergo episodes of forward movement at $v = \bar{v}_{max}$ interrupted by episodes of diffusion with zero average velocity, so that over the entire trajectory the mean $\bar{v} < \bar{v}_{max}$. Some examples of such alternation between directed and random movement could be identified visually in experiments at very low K448−BIO surface density when methylcellulose was present. Microtubules underwent directed movement through a pivot point, but when the trailing microtubule end passed through its attachment point, the microtubule diffused randomly over the surface until it formed another attachment to the surface and resumed unidirectional movement. The length of a directed movement episode will depend on the number of molecules participating during the episode and on the processivity of the motor (expected to be high in methylcellulose). In the microtubule gliding assay, intact kinesin displays complete processivity so that, even in the absence of methylcellulose, episodes driven by a single molecule will last until the end of the microtubule is reached (*11*).

The distinctive episodic behavior of the high duty ratio model differs from that predicted by a low duty ratio model, which posits that an active motor molecule participating in microtubule movement spends significant time during its enzymatic cycle in reaction steps that do not produce movement ("nonproductive" steps). No forward movement occurs during intervals when all participating motor molecules are in nonproductive steps, but such intervals will be rarer and shorter (and velocity v will be higher) for a large number of participating molecules than for a small number. Thus, v can take on a variety of values between 0 (no motors participating) and $\bar{v}_{max}$ (continuous movement, when the number of participating molecules is sufficiently large). For a sufficiently low surface density of motor molecules, v will exhibit small fluctuations but will remain uniformly less than $\bar{v}_{max}$ (assuming as always that the time resolution w is significantly longer than the enzymatic cycle time). We stress that both the high duty ratio model and the low duty ratio model predict that, at sufficiently low surface density of motors, trajectories with submaximal mean velocity ($\bar{v} < \bar{v}_{max}$) will be observed. However, only the high duty ratio model predicts that such trajectories contain episodic fluctuation of instantaneous velocity v between movement at $\bar{v}_{max}$ and undirected movement. Detection of such episodic behavior is the goal of our analysis, but isolated maximal-velocity movement events are difficult to identify individually because diffusion of microtubules when not attached to motors introduces substantial fluctuations into v. Therefore, our analysis takes into account all values of v from trajectories with submaximal $\bar{v}$.

One simple approach to duty ratio measurement is distribution analysis: a histogram is constructed from all values of instantaneous velocity v from a pool of trajectories with a narrow range of $\bar{v}$ values all significantly less than $\bar{v}_{max}$. Trajectories with episodic fluctuations predicted by a high duty ratio model should have values of v clustered around $\bar{v}_{max}$ and around 0 rather than in between. Distribution analysis does not explicitly measure the duration of episodes with $v \approx \bar{v}_{max}$, except to show that they are long enough to be detected.

An alternative analytical method, autocovariance analysis, complements distribution analysis by recognizing that within an episode of continuous high-velocity movement the individual values of v should be mutually correlated (autocorrelated). Consequently, there should be a significant probability that v measured at any time t during the trajectory is similar in value to v measured some time interval τ before or after t. The autocovariance analysis for v used in this work measures the temporal autocorrelation of $(v - \bar{v})/(\bar{v}_{max}/2)$ for trajectories with submaximal $\bar{v}$. In general the autocovariance will have a large positive value for $\tau \approx 0$ but will fall to zero when τ approaches the typical duration of episodes with v significantly greater (or smaller) than $\bar{v}$. This duration should be of detectable magnitude in trajectories generated by a high duty ratio motor, unless processivity of movement is reduced by prolonged detachments of

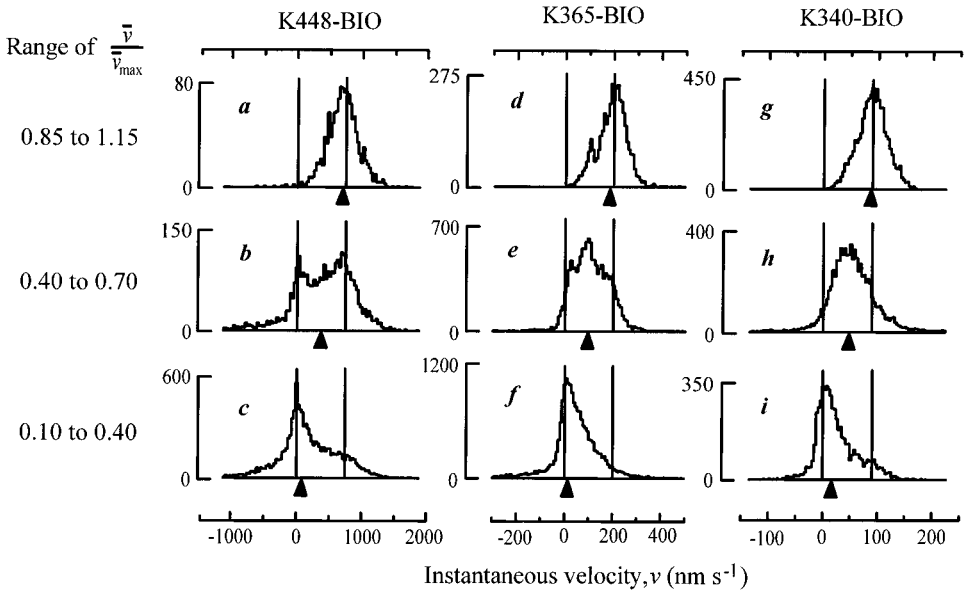

FIGURE 3: Distributions of instantaneous longitudinal velocities in microtubule trajectories at 1 mM ATP. Each column of three histograms shows data from one kinesin derivative as indicated by the column heading. Each histogram in a column shows data pooled from microtubule trajectories for which $\bar{v}/\bar{v}_{max}$ falls within the limits indicated at the left side of the figure. Instantaneous velocities were calculated using the time window width w selected individually for each derivative (see Materials and Methods). For K448−BIO (a−c), $\bar{v}_{max} = 750$ nm s^{-1}, $w = 650$ ms; for K365−BIO (d−f), $\bar{v}_{max} = 200$ nm s^{-1}, $w = 5000$ ms; for K340−BIO (g−i), $\bar{v}_{max} = 90$ nm s^{-1}, $w = 6000$ ms. Vertical scales indicate the number of data points in bins of width $0.04\bar{v}_{max}$. The positions of 0 and $\bar{v}_{max}$ on the horizontal axes are marked with vertical lines; arrowheads indicate the positions of the mean value of each distribution.

the motor from the microtubule. In contrast, trajectories generated by a low duty ratio motor, in which v is predominantly close to $\bar{v}$ and less than $\bar{v}_{max}$, will have much smaller autocovariance except for τ values so small as to approach the enzymatic cycle time. Similarly, microtubules freely diffusing should also show no significant autocovariance at the values of τ measured here because diffusional correlation time for a microtubule under these conditions is $\ll 1$ μs (*34*).

Distribution Analysis of Instantaneous Velocities. For a high duty ratio motor, the histogram of v values in trajectories with submaximal $\bar{v}$ should show two peaks, at 0 and $\bar{v}_{max}$. However, these peaks can only be resolved if they are sufficiently narrow relative to the distance between them ($\bar{v}_{max}$). Peak broadening can arise through the underlying variation in the instantaneous microtubule velocity or through random errors in measuring the velocity v. One source of error in v is random scatter introduced through errors in measuring microtubule position ("position-error noise"). This scatter will be of constant magnitude, so the resultant peak broadening relative to $\bar{v}_{max}$ will be more pronounced if $\bar{v}_{max}$ is low than if $\bar{v}_{max}$ is high. Scatter can be suppressed through time-averaging, such as by increasing the duration w of the short time window used to calculate v. However, the length of the time window limits the time resolution for detecting changes in velocity; in effect, fluctuations in v are low-pass filtered. Near the beginning and end of motor-driven movement episodes, filtering would cause v to have a value intermediate between the true values of 0 and $\bar{v}_{max}$. Thus, for our distribution analysis, w should be the shortest time window that sufficiently suppresses position-error noise and will be specific to a given motor; w must be longer for a motor with low $\bar{v}_{max}$. For each motor, a number of different w values were used in turn for calculating v values in trajectories of continuous gliding at $\bar{v} \approx \bar{v}_{max}$. Then the smallest w giving a narrow distribution of v values (sd $\leq$ $\bar{v}_{max}/3$) was selected. This selection fixed the value of w for subsequent calculations of v in the motor's intermediate and low $\bar{v}/\bar{v}_{max}$ trajectories; after w is fixed, there are no adjustable parameters in the calculation of v from position data.

Figure 3 shows histograms of v constructed from all trajectories in high, intermediate, and low $\bar{v}/\bar{v}_{max}$ pools. For K448−BIO, a time window $w = 650$ ms gave sufficient noise suppression in the single peak at $\bar{v}_{max}$ in the velocity histogram from the high $\bar{v}/\bar{v}_{max}$ pool (Figure 3a), and also fulfilled the requirement that $w \gg$ the enzymatic turnover time of 10 ms. The histograms for intermediate or low $\bar{v}/\bar{v}_{max}$ pools (Figure 3b,c) show that, in K448−BIO experiments, v values are distributed around either 0 or $\bar{v}_{max}$, as expected from the high duty ratio model. This is in contrast to K340−BIO and K365−BIO experiments, for which the histograms from intermediate or low $\bar{v}/\bar{v}_{max}$ pools are unimodal, centered near $\bar{v}$ (Figure 3e,f,h,i). Longer time windows ($w = 5$ or 6 s) were used for calculating v of the monomeric motors to ensure that the relative extent of suppression of positional-error noise would be comparable to that obtained for K448−BIO in Figure 3b. Successful noise suppression is confirmed by the histograms for high $\bar{v}/\bar{v}_{max}$ pools of the three motors (Figure 3a,d,g), which all have similar width when normalized for the differences in $\bar{v}_{max}$. Therefore the unimodal distributions in intermediate or low $\bar{v}/\bar{v}_{max}$ trajectory pools for monomeric motors do not result from superimpositions of two unresolved peaks at 0 and $\bar{v}_{max}$. Rather, in such trajectories v takes values predominantly near $\bar{v}$, intermediate between 0 and $\bar{v}_{max}$, which is inconsistent with movement generated by a processive motor with high duty ratio like kinesin.

Autocovariance Analysis of Instantaneous Velocities. Autocovariance analysis was performed on pools of trajectories with $0.4 \leq \bar{v}/\bar{v}_{max} \leq 0.7$ (the same as the intermediate $\bar{v}/\bar{v}_{max}$ pool treated in distribution analysis). First, $v(t)$ was

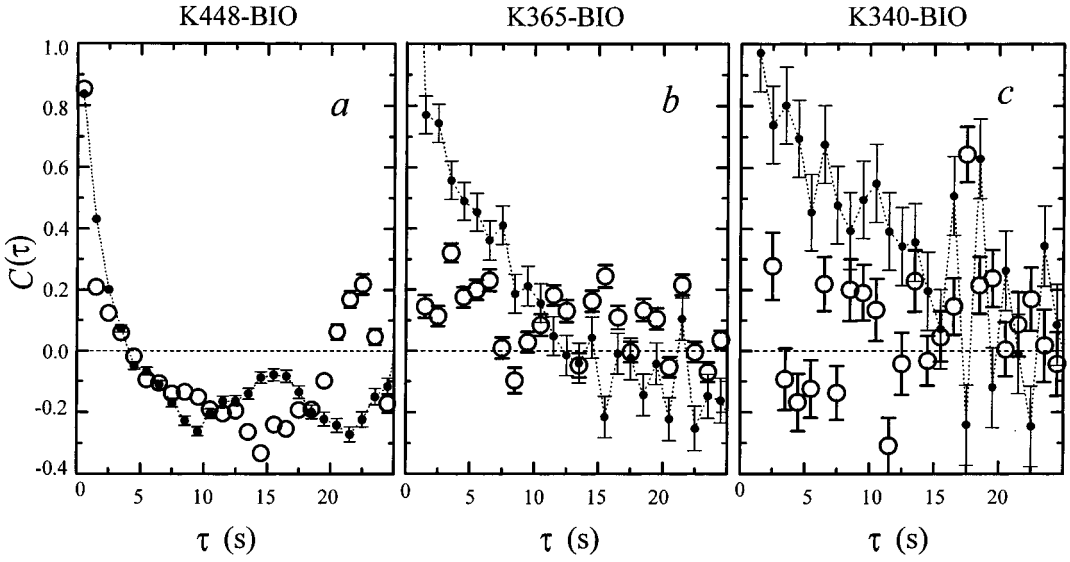

FIGURE 4: Temporal autocovariances of instantaneous longitudinal velocities from trajectories with submaximal average velocity. Points show mean value (±se) of the autocovariance $C(\tau)$ evaluated in bins of 1 s (see Materials and Methods), for trajectories with $0.40 \leq \bar{\nu}/\bar{\nu}_{max} \leq 0.70$, either observed in experiments on kinesin derivatives (○, unconnected) or produced by simulation (see Materials and Methods) of a high duty ratio motor with complete processivity (●, connected). The experimental trajectories were the same as those analyzed in Figure 3b,e,h; the simulated trajectories used $\bar{\nu}_{max}$ specific to each motor (Figure 3 caption) and longitudinal microtubule diffusion coefficient $D_{long} = 1 \times 10^4$ nm^2 s^{-1}. Instantaneous velocity was calculated using the time window $w = 500$ ms for all trajectories.

divided by $\bar{\nu}_{max}/2$ and its autocovariance evaluated for each trajectory. The individual trajectory autocovariances from a pool were then averaged together, weighted by trajectory length, to give the average autocovariance $C(\tau)$ for that pool. We expected that, for correlation time intervals τ near zero, $C(\tau)$ would have a high value whether the trajectories were generated by high or low duty ratio motors. The difference between $C(\tau)$ for high and for low duty ratio trajectories should be most prominent for larger values of the correlation time interval τ. Since the effects of high-frequency noise (such as that arising from position-error noise) are smallest at large τ, the autocovariance analysis has a less stringent requirement for noise suppression than does the distribution analysis. Hence, a shorter time window w of 500 ms was used in calculations of ν for all three motors; this time window is still larger than the enzymatic turnover time as required (see *Rationale for Duty Ratio Measurement Techniques*).

The autocovariance curve for K448−BIO (Figure 4a, open points) had significant negative values for $\tau \geq 4$ s. The negative correlation indicates that if ν is much greater than $\bar{\nu}$ at a given time t, values of ν at 4 s or more before or after t tend to be much less than $\bar{\nu}$, rather than randomly distributed above and below $\bar{\nu}$. This means that each high-velocity episode is typically preceded and followed by low-velocity episodes of several seconds duration. Conversely, each low-velocity episode tends to be flanked by long high-velocity episodes. Since the typical duration of high-velocity episodes is on the order of the time required for a motor molecule to move to the end of the microtubule at speed $\bar{\nu}_{max}$, the K448−BIO autocovariance curve appears consistent with that of a "completely" processive motor. Complete processivity implies that the motor in the gliding assay invariably remains associated with the microtubule until it reaches the microtubule end, as is observed with intact kinesin (*11*).

The interpretation of the autocovariance curve was tested by numerical simulation of longitudinal displacement trajectories for a model of a completely processive, high duty ratio motor model with $\bar{\nu}_{max} = 750$ s^{-1}. In each simulated trajectory, a microtubule of randomly chosen length L underwent several episodes of directed movement at speed $\bar{\nu}_{max}$, alternating with episodes of diffusion. Directed movement episodes were assumed to begin with initial attachment of the motor at a random position along the microtubule and to last until the motor moved to the plus-end of the microtubule. Simulated trajectories were analyzed by an autocovariance procedure identical to that used for the experimental data, so that the experimental results could be directly compared with those from the model. The two autocovariance curves are remarkably similar; both cross the horizontal axis near $\tau = 4$ s and show significant negative correlations in the $\tau > 4$ s region. Thus, the autocovariance curve for experimental K448−BIO trajectories is consistent with the complete processivity/high duty ratio model.

The same strategy used for interpreting autocovariance curves of K448−BIO was applied to the monomeric motors, by repeating the simulations with the modification that the value of $\bar{\nu}_{max}$ was 200 (as for K365−BIO) or 90 nm s^{-1} (as for K340−BIO). That is, these simulations represented models in which the monomeric motors are completely processive and have high duty ratio. The $C(\tau)$ curves from the simulations displayed negative correlation similar to that seen previously with $\bar{\nu}_{max} = 750$ nm s^{-1}, but with horizontal axis intercepts at $\tau \approx 15$ s for $\bar{\nu}_{max} = 200$ nm s^{-1} and at $\tau \approx 30$ s for $\bar{\nu}_{max} = 90$ nm s^{-1}. (The progressive shift in the intercept as $\bar{\nu}_{max}$ decreased reflects the increase in the time required for a motor to reach the microtubule end in the complete processivity/high duty ratio model.) For both K365−BIO (Figure 4b) and K340−BIO (Figure 4c), the autocovariance curves from experimental data (open points) clearly departed from the corresponding simulations (solid points and dashed curve), indicating that the movement generated by the monomeric kinesin derivatives is not consistent with a completely processive, high duty ratio

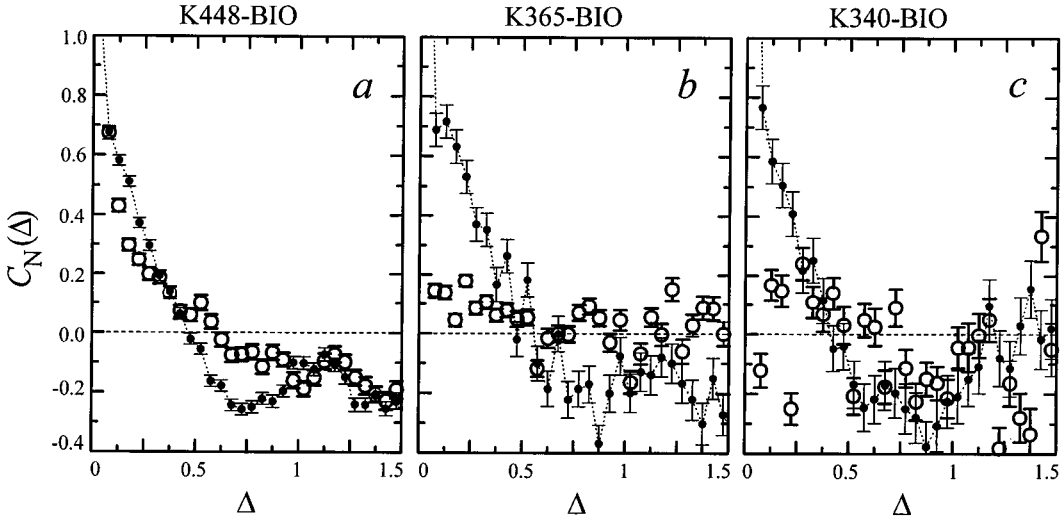

FIGURE 5: Length-normalized autocovariances of instantaneous longitudinal velocities. Analysis was performed on the same experimental (○, unconnected) and simulated (●, connected) trajectory pools as those in Figure 4, with $w = 500$ ms. Time scales of data sets were rescaled according to microtubule length in each trajectory (see Materials and Methods). Horizontal scale is the dimensionless parameter Δ (see Materials and Methods); a value of $\Delta = 1$ corresponds to the time required to move the full microtubule length (L) at velocity $\bar{\nu}_{max}$.

model. The scatter in both simulation and experimental curves, and the off-scale values for the autocovariances at $\tau < 1$ s, can be attributed to position-error noise, which has a more prominent effect relative to the low $\bar{\nu}_{max}$ of the monomeric motors. When noise was suppressed by calculating ν with a larger w, both curves were smoothed and the values at $\tau < 1$ s were decreased; the values at $\tau > 1$ s were not affected (not shown).

Neither K340−BIO nor K365−BIO experimental autocovariances had consistently positive or negative values for $\tau > 5$ s. This shows that fluctuations of ν between values much greater or much less than $\bar{\nu}$, if present at all, must occur at higher frequency than in the case of K448−BIO trajectories. For $\tau < 5$ s, there was a consistent small positive correlation in the K365−BIO experimental curve with magnitude ~0.2. However, this indicates a typical departure of ν no more than $(0.2^{1/2})\bar{\nu}_{max}/2 = 0.07\bar{\nu}_{max}$ away from its mean value of $\sim 0.55\bar{\nu}_{max}$.

For a given microtubule in the motility assay, the mean duration of the episodes of directed movement at $\nu = \bar{\nu}_{max}$ by a completely processive motor is predicted to be $0.5L/\bar{\nu}_{max}$, where L is the microtubule length. (The coefficient 0.5 is due to the fact that such motors are expected to bind to the microtubule initially at a random location on its length and then to move all the way to the microtubule plus-end; the mean distance traveled in such an episode is $0.5L$.) To test whether experimental trajectory data fulfilled this prediction, the time variable t_i of each trajectory's data set was normalized by dividing it by $L/\bar{\nu}_{max}$, for the values of L and $\bar{\nu}_{max}$ specific to that trajectory. This converted the independent variable to the dimensionless $\delta_i = t_i\bar{\nu}_{max}/L$. The resultant "length-normalized" data sets were then used to recalculate autocovariance curves with respect to δ-intervals rather than time intervals. A δ-interval of $\Delta = 0.5$ corresponds to a time interval of $0.5L/\bar{\nu}_{max}$, the expected mean episode duration of a completely processive, high duty ratio motor. The normalized autocovariance $C_N(\Delta)$ curves derived from the simulations of such a motor (Figure 5) all crossed zero at $\Delta = 0.5$ as expected.

The microtubule-length-normalized autocovariance $C_N(\Delta)$ of K448−BIO experimental trajectories also showed negative correlation at $\Delta > 0.5$, matching the curves from the simulations (Figure 5a). Thus, the K448−BIO experimental data can be interpreted as episodes of motor-driven movement limited only by microtubule length, alternating with episodes of diffusion free of motor attachment. In contrast, $C_N(\Delta)$ curves for K365−BIO and K340−BIO experimental trajectories were close to zero for even small values of Δ and had no negative correlation (Figure 5b,c). We considered that combining data from experimental trajectories in a pool would be biased if many trajectories had net displacement much smaller than a microtubule length. However, there is no evidence for such bias because the results were unchanged if all experimental trajectories with net displacement $<0.5L$ were discarded (not shown). Therefore the autocovariance analysis reinforces the conclusions of the distribution analysis: the two-headed K448−BIO has a high duty ratio and a processivity that appears to be complete, like intact kinesin, while the one-headed K365−BIO and K340−BIO have movement inconsistent with high duty ratio and high processivity.

DISCUSSION

In this work, the addition of methylcellulose to the microtubule gliding assay enabled us to study movement driven by small numbers of motor molecules, even for motors which do not maintain continuous association with microtubules. Without methylcellulose, microtubules move laterally (i.e., in directions perpendicular to the microtubule long axis) by random thermal motion and do not remain near the surface. Methylcellulose at a concentration of 0.07% forms a loose three-dimensional network that effectively prevents this lateral motion, particularly in the direction perpendicular to the coverslip surface. However, methylcellulose has much less effect on longitudinal movement (parallel to the long axis). Thus, as in previous studies with actin filaments (*9*), microtubules can be observed continuously moving over surfaces on which motors are present at very low density, such that the initial encounter of a microtubule with a motor may be rare. Diffusive movements (which occur while the microtubule is not attached to any motor) are incorporated

along with motor-driven movements into one continuous microtubule trajectory.

Surface density of motor molecules in the gliding assay is controlled by adjusting the concentration of motor in the solution applied to the coverslip in a fixed incubation time, but our approach does not require direct measurement of the density. Previous duty ratio studies of myosin and dynein in the filament gliding assay depended on quantitative correlations of mean velocity in a trajectory ($\bar{\nu}$) with the estimated number of motor molecules producing movement, with no distinctions made between episodic or uniform movement within such trajectories. In those studies the average density of motor molecules on the coverslip surface was found from the ATPase activity (*9*) or by electron microscopy (*10*), but this value can be misleading since the local motor density producing a microtubule trajectory in a given region of the coverslip might be considerably below or above the average. Moreover, different motor molecules might contact a filament with varying geometries, not all of which are equally suitable for contributing to movement. Our analysis measures the fluctuations in velocity within trajectories and does not depend on knowledge of the number of motor molecules contributing to movement at any individual point in a trajectory.

The monomeric and dimeric kinesin derivatives in this work are all recombinant biotinated fusion proteins and thus can be attached specifically (*22*) to a streptavidin-coated coverslip. This reduces the probability that the kinesin moieties of the fusion proteins suffer steric interference from direct contact with the coverslip (*16*, *24*). The uniform orientation of attachment to the surface facilitates comparison of the different motors' motility at low surface density. To allay concerns that differences between K340−BIO and K448−BIO (*22*) might arise solely because of interactions of the motor domain with the adjacent biotinated domain in K340−BIO, we tested the monomeric K365−BIO, which has 25 additional kinesin residues between the motor domain and the biotin acceptor domain. We found that both monomers K340−BIO and K365−BIO differ markedly from dimeric K448−BIO in duty ratio.

When K448−BIO is attached to surfaces at low density, microtubule movement through single pivot points of attachment to the surface can be observed. We have not shown rigorously in this work that pivoting events arise from the action of single K448−BIO dimers, but the pivoting is similar to that seen for single molecules of intact kinesin (*11*). If all K448−BIO dimers in solution bound to the surfaces of the $\sim 20 \times 3 \times 0.1$ mm flow cell and were active, incubation of the cell with a 0.1 nM solution of motor would produce a mean active motor density of ~ 5 molecules μm^{-2}. Then a microtubule of length 1−15 μm and diameter 25 nm would interact with only one or two active motors at once on average, so attribution of pivoting to single molecules of K448−BIO is plausible. This would augment the list of properties of intact kinesin which are successfully mimicked by the rodless truncation mutant K448−BIO: the list also includes microtubule-stimulated ATPase activity, stable self-association (*20*), and single-molecule motility in the enzyme-linked bead assay (*21*) with discrete 8 nm steps (*23*) and high fidelity to the microtubule protofilament axis (*22*). We stress, however, that the analyses in this work do not rely on identification of isolated movement episodes such as microtubule pivoting events. Rather, trajectories with submaximal mean velocity are treated in their entirety.

Movement generated at low densities of two-headed K448−BIO fits in all respects a model of a completely processive, high duty ratio motor. Within K448−BIO-driven trajectories with mean longitudinal velocity $\bar{\nu} < \bar{\nu}_{max}$, distribution analysis detects coexistence of two distinct modes of microtubule movements: undirected and directed. This provides positive evidence that the number of contributing K448−BIO molecules is not equally large at all points in these trajectories and sometimes drops to zero. The velocity of directed movement in these trajectories (the peak in the distribution at 750 nm s^{-1}, Figure 3b) matches the $\bar{\nu}_{max}$ for K448−BIO found in trajectories of continuous gliding driven by large numbers of K448−BIO molecules (Figure 3a). The $\bar{\nu}_{max}$ for gliding also replicates the velocity of K448−BIO at 1 mM ATP in the bead assay (*23*). Episodes of directed movements at speeds significantly less than $\bar{\nu}_{max}$ are not observed; thus, K448−BIO has a duty ratio near unity. Autocovariance analysis shows that within intermediate $\bar{\nu}/\bar{\nu}_{max}$ trajectories, the duration of sustained forward movement is limited by microtubule length. This is consistent with intermittent encounters of the microtubule with single molecules of a completely processive motor on a sparsely coated surface. Simulations of this model are consistent with the experimental data, provided that microtubules interacting with K448−BIO-coated surfaces have a somewhat lower diffusion coefficient than those above motor-free surfaces (see Materials and Methods, *Estimates of Microtubule Diffusion Coefficient*).

The one-headed kinesin derivatives K340−BIO and K365−BIO display $\bar{\nu}_{max}$ values at high motor density which are lower than the $\bar{\nu}_{max}$ values of K448−BIO and of intact kinesin; the discrepancy exists whether or not methylcellulose is present. Other presumptively monomeric motors derived from the kinesin motor domain all drive movement in the microtubule gliding assay at low velocities like K340−BIO and K365−BIO (*24*, *27*, *37*−*39*). Our estimates of $\bar{\nu}_{max}$ for K340−BIO and K365−BIO were made by inspection of saturating values for $\bar{\nu}$ in Figure 2b,c. Even if the true $\bar{\nu}_{max}$ of either of these motors is higher than the estimated value used in this work, the conclusions of the distribution and autocovariance analyses will still hold: in trajectories generated at low density for which $\bar{\nu} = \sim\bar{\nu}_{max}/2$, instantaneous velocity ν is predominantly less than $\bar{\nu}_{max}$. There is no evidence in such trajectories for lengthy episodes during which the microtubule is detached from all motors or during which the microtubule moves at $\bar{\nu}_{max}$. Thus, both K340−BIO and K365−BIO fail to display the properties of a highly processive, high duty ratio motor.

The number of participating motors producing intermediate $\bar{\nu}/\bar{\nu}_{max}$ trajectories might be more than one for K340−BIO or K365−BIO, since for most of these trajectories the nominal surface density of motors (assuming all molecules attached and were active) was ~ 50 μm^{-2} or higher. If multiple molecules were indeed interacting with the microtubule, we must consider the possibility that one motor molecule could become rigidly attached to the microtubule and suppress the movement generated by other molecules (as for smooth muscle myosin (*13*)). Formation of a rigid attachment might or might not be part of the normal turnover cycle. Stable complexes between monomeric motors and

microtubules do form when ATP is scarce, as shown by the attachment of microtubules to motor-coated surfaces in 50 nM ATP; stable nucleotide-free complexes are also seen for intact kinesin (*1*, *40*) and at low ATP multiple kinesin molecules produce lower velocity than single kinesin molecules (*11*). However, at the 1 mM concentration of ATP used in our observations of motility, K340−BIO appears not to form any rigid attachment to microtubules that hinders movement. Such attachments would cause velocity to decrease with increased surface density, as the inhibitory attachments of motors to microtubules became more frequent, and this is not seen for K340−BIO gliding. (For K365−BIO there are fewer data at high surface densities to support this argument.) We conclude that during any steps of K340−BIO's cycle that do not generate forward movement, K340−BIO molecules on the surface must be either detached from the microtubule or else attached to the microtubule by a flexible linkage. Moreover, if multiple K340−BIO molecules produced the intermediate $\bar{v}/\bar{v}_{max}$ trajectories with average velocity 0.55 $\bar{v}_{max}$, then a single K340−BIO molecule must drive movement with speed significantly less than 0.55 $\bar{v}_{max}$. Therefore the duty ratio is significantly less than 55%; note, however, that the processivity of the motor may be high or low.

We turn to models in which single molecules produce the trajectories. One model consistent with our data is that a single monomeric motor molecule is highly processive in our assay with methylcellulose, yet drives movement with velocity less than $\bar{v}_{max}$ in the presence of methylcellulose. The low velocity from a single molecule is likely not due to the effects of frictional drag on the microtubule, because drag should increase with microtubule length, and the experimental values of $\bar{v}$ were independent of length. Therefore in this model the duty ratio of the monomer is ≈55% (the average value of $\bar{v}/\bar{v}_{max}$ in the trajectories). This duty ratio is significantly smaller than intact kinesin's duty ratio near 100%.

While the above two models both imply that the duty ratio is 55% or less, there is an unusual alternative model which our data do not exclude, in which the duty ratio may be high. In this model, a single monomer has low processivity in our assay despite the presence of methylcellulose, because it enters a prolonged state in which it cannot attach to a microtubule (the state might or might not be part of normal turnover). Then a single monomer might drive short episodes of movement near $\bar{v}_{max}$ (a high duty ratio), but the fluctuation between high and low velocity within intermediate $\bar{v}/\bar{v}_{max}$ trajectories might be too fast for detection with the time resolution of our analysis. If we estimate that the shortest detectable high-velocity run is approximately half the value of $w = 5$ or 6 s used in distribution analysis, then the monomer's processivity must be no more than approximately 600 nm in the case of K365−BIO and even less in the case of K340−BIO. In the absence of methylcellulose the processivity is expected to be even less. This is in contrast to intact kinesin, which even without methylcellulose produces complete processivity in the gliding assay (*11*).

Our experiments in the absence of methylcellulose show that interaction of microtubules with one-headed motors at low densities is interrupted frequently by intervals during which no motors are attached to the microtubule. The attachment-free intervals are long enough that there is a high probability that the microtubule will diffuse a critical "escape" distance from the motors, unless the methylcellulose network is present to suppress lateral diffusion. Thus, we can exclude models of monomeric kinesin movement in which the motor "slides" along a continuum of binding sites on the microtubule (*41*) for long distances without ever becoming detached. Even though K448−BIO is highly processive, there is evidence that this dimeric motor also detaches from the microtubule during movement at least occasionally, if not in every turnover cycle. In the gliding assay in this work, K448−BIO gliding run distance appears limited only by the microtubule length (∼4 μm on average), while in previous studies with the bead assay the single-molecule K448−BIO run distance was only ≤1 μm (*23*, *42*). The difference in run distance between the gliding and bead assays exactly duplicates that seen for intact kinesin (*11*, *12*) and reflects the difference between diffusion coefficients for a microtubule and for a 100 nm diameter bead, as well as the higher density of sites for motor-microtubule attachment presented by the surface of a free microtubule relative to that of an enzyme-conjugated bead (*12*). Detachment would result in termination of movement only in the event that the motor and microtubule diffused away from each other before reattachment, which is more likely for the bead assay than for the gliding assay. A plausible mechanism for two-headed K448−BIO movement that explains both high processivity and occasional detachment from microtubules is that each of its component heads undergoes a cycle of attachment to and detachment from the microtubule, most likely in a coordinated fashion. A state in which both heads are detached would have a low probability of occurring and/or a short lifetime, but cannot be altogether avoided.

The isolated head of myosin (S1) is a nonprocessive motor (*43*), and incorporation of two S1 heads into a dimeric molecule (HMM) does not produce a processive motor with high duty ratio (*9*, *44*). We have demonstrated that two distinct monomeric derivatives (K340−BIO and K365−BIO) containing the kinesin motor domain resemble myosin rather than intact kinesin, in having a low duty ratio or low processivity or both. Yet the two-headed derivative K448−BIO displays the high processivity and high duty ratio of intact kinesin. While we have not investigated any one-headed derivative containing a complete set of neck residues, the part of the kinesin neck sequence in K365−BIO is certainly insufficient to confer high duty ratio processive movement to the monomeric motor domain. The data suggest that the key requisite for kinesin's movement with high duty ratio and high processivity is the association of two motor domains in the same motor molecule.

One-headed kinesins differ from two-headed kinesins in other ways: K340−BIO fails to follow the protofilament axis (*22*); the number of ATP hydrolytic events associated with a diffusional encounter with a microtubule is far lower for monomeric than for dimeric derivatives (*7*, *45*, *46*), and dimers but not monomers display half-sites reactivity in microtubule-stimulated nucleotide release (*17*). Essentially all existing comparisons of one- and two-headed kinesins are consistent with simple alternating sites mechanisms for intact two-headed kinesin (*17*, *18*) in which functional coordination of the two heads is required for processive, high duty ratio movement. It is not known if simple physical linkage of heads may be sufficient for such coordination or

if specific interactions (e.g., in the neck region) are required. The gliding assay and the analysis developed in this work are useful tests of motor mechanism applicable to either processive or nonprocessive motors. Biotinated recombinant two-headed motors engineered to have heads in different spatial relationships would be promising candidates for further application of these methods.

ACKNOWLEDGMENT

We thank D. Decker and L. Khainson for technical assistance, I. Hristov for software, and H. Huxley for comments on a preliminary manuscript.

REFERENCES

1. Vale, R. D., Reese, T. S., and Sheetz, M. P. (1985) *Cell 42*, 39−50.
2. Kron, S. J., and Spudich, J. A. (1986) *Proc. Natl. Acad. Sci. U.S.A. 83*, 6272−6276.
3. Sheetz, M. P., and Spudich, J. A. (1983) *Nature 303*, 31−35.
4. Funatsu, T., Harada, Y., Tokunaga, M., Saito, K., and Yanagida, T. (1995) *Nature 374*, 555−559.
5. Huxley, H. E. (1969) *Science 164*, 1356−1366.
6. Lymn, R. W., and Taylor, E. W. (1971) *Biochemistry 10*, 4617−4624.
7. Hackney, D. D. (1995) *Nature 376*, 215−216.
8. Howard, J. (1997) *Nature 389*, 561−7.
9. Uyeda, T. Q. P., Kron, S. J., and Spudich, J. A. (1990) *J. Mol. Biol. 214*, 699−710.
10. Hamasaki, T., Holwill, M. E., Barkalow, K., and Satir, P. (1995) *Biophys. J. 69*, 2569−79.
11. Howard, J., Hudspeth, A. J., and Vale, R. D. (1989) *Nature 342*, 154−158.
12. Block, S. M., Goldstein, L. S. B., and Schnapp, B. J. (1990) *Nature 348*, 348−352.
13. Warshaw, D. M., Desrosiers, J. M., Work, S. S., and Trybus, K. M. (1990) *J. Cell. Biol. 111*, 453−463.
14. Hirokawa, N., Pfister, K. K., Yorifuji, H., Wagner, M. C., Brady, S. T., and Bloom, G. S. (1989) *Cell 56*, 867−878.
15. Scholey, J. M., Heuser, J., Yang, J. T., and Goldstein, L. S. B. (1989) *Nature 338*, 355−357.
16. Yang, J. T., Saxton, W. M., Stewart, R. J., Raff, E. C., and Goldstein, L. S. B. (1990) *Science 249*, 42−47.
17. Hackney, D. D. (1994) *Proc. Natl. Acad. Sci. U.S.A. 91*, 6865−6869.
18. Gelles, J., Berliner, E., Young, E. C., Mahtani, H. K., Perez-Ramirez, B., and Anderson, K. (1995) *Biophys. J. 68*, 276s−282s.
19. Hackney, D. D., Levitt, J. D., and Wagner, D. D. (1991) *Biochem. Biophys. Res. Commun. 174*, 810−815.
20. Young, E. C., Berliner, E., Mahtani, H. K., Perez-Ramirez, B., and Gelles, J. (1995) *J. Biol. Chem. 270*, 3926−3931.
21. Berliner, E. (1995) Ph.D. Thesis, Brandeis University.
22. Berliner, E., Young, E. C., Anderson, K., Mahtani, H. K., and Gelles, J. (1995) *Nature 373*, 718−721.
23. Hua, W., Young, E. C., Fleming, M. L., and Gelles, J. (1997) *Nature 388*, 390−393.
24. Stewart, R. J., Thaler, J. P., and Goldstein, L. S. B. (1993) *Proc. Natl. Acad. Sci. U.S.A. 90*, 5209−5213.
25. Huang, T.-G., and Hackney, D. D. (1994) *J. Biol. Chem. 269*, 16493−16501.
26. Huang, T.-G., Suhan, J., and Hackney, D. D. (1994) *J. Biol. Chem. 269*, 16502−16507.
27. Vale, R. D., Funatsu, T., Pierce, D. W., Romberg, L., Harada, Y., and Yanagida, T. (1996) *Nature 380*, 451−453.
28. Young, E. C., and Gelles, J. (1997) *Biophys. J. 72*, A235.
29. Berliner, E., Mahtani, H. K., Karki, S., Chu, L. F., Cronan, J. E., Jr., and Gelles, J. (1994) *J. Biol. Chem. 269*, 8610−8615.
30. Kohanski, R. A., and Lane, M. D. (1990) *Methods Enzymol. 184*, 194−200.
31. Englander, S. W., and Crowe, D. (1965) *Anal. Biochem. 12*, 579−584.
32. Gelles, J., Schnapp, B. J., and Sheetz, M. P. (1988) *Nature 331*, 450−453.
33. Nakata, T., Sato-Yoshitake, R., Okada, Y., Noda, Y., and Hirokawa, N. (1993) *Biophys. J. 65*, 2504−2510.
34. Berg, H. C. (1993) *Random Walks in Biology*, expanded ed.; Princeton University Press, Princeton, NJ.
35. Hunt, A. J., Gittes, F., and Howard, J. (1994) *Biophys. J. 67*, 766−781.
36. Kull, F. J., Sablin, E. P., Lau, R., Fletterick, R. J., and Vale, R. D. (1996) *Nature 380*, 550−555.
37. Ramanathan, K., and Kuo, S. C. (1996) *Biophys. J. 70*, 37a.
38. Hancock, W. O., and Howard, J. (1997) *Biophys. J. 72*, A61.
39. Inoue, Y., Toyoshima, Y. Y., Iwane, A. H., Morimoto, S., Higuchi, H., and Yanagida, T. (1997) *Proc. Natl. Acad. Sci. U.S.A. 94*, 7275−7280.
40. Romberg, L., and Vale, R. D. (1993) *Nature 361*, 168−170.
41. Vale, R. D., and Oosawa, F. (1990) *Adv. Biophys. 26*, 97−134.
42. Vugmeyster, Y., Berliner, E., and Gelles, J. (1997) *Biochemistry 37*, 747−757.
43. Molloy, J. E., Burns, J. E., Kendrick-Jones, J., Tregear, R. T., and White, D. C. S. (1995) *Nature 378*, 209−212.
44. Finer, J. T., Simmons, R. M., and Spudich, J. A. (1994) *Nature 368*, 113−119.
45. Jiang, W., Stock, M. F., Li, X., and Hackney, D. D. (1997) *J. Biol. Chem. 272*, 7626−7632.
46. Ma, Y.-Z., and Taylor, E. W. (1997) *J. Biol. Chem. 272*, 717−723.

BI972172N